

Super-resolution correlative light-electron microscopy using a click-chemistry approach for studying intracellular trafficking

**Teodora Andrian^{a,†}, Thomas Bakkum^{b,†}, Daphne M. van Elsland^c, Erik Bos^d,
Abraham J. Koster^d, Lorenzo Albertazzi^{a,e,*}, Sander I. van Kasteren^{b,*},
and Sílvia Pujals^{a,f,*}**

^a*Institute of Bioengineering of Catalonia (IBEC), Barcelona Institute of Science and Technology,
Barcelona, Spain*

^b*Leiden Institute of Chemistry and The Institute for Chemical Immunology, Leiden University,
Leiden, The Netherlands*

^c*Department of Cell and Chemical Biology, The Institute for Chemical Immunology, Leiden
University Medical Center LUMC, Leiden, The Netherlands*

^d*Department of Cell and Chemical Biology, Section Electron Microscopy, Leiden University
Medical Center LUMC, Leiden, The Netherlands*

^e*Department of Biomedical Engineering, Institute of Complex Molecular Systems, Eindhoven
University of Technology, Eindhoven, The Netherlands*

^f*Department of Electronics and Biomedical Engineering, Faculty of Physics, Universitat de
Barcelona, Barcelona, Spain*

**Corresponding authors: e-mail address: lalbertazzi@ibecbarcelona.eu;
s.i.van.kasteren@chem.leidenuniv.nl; spujals@ibecbarcelona.eu*

Chapter outline

1 Introduction.....	305
1.1 CLEM and super-resolution microscopy.....	305
1.2 SMLM-CLEM, advantages over conventional CLEM.....	305

[†]These authors contributed equally to this work.

1.3	Fixation in SRM-CLEM.....	306
1.4	Fluorescence labeling: Advantages of click chemistry.....	307
1.5	Case study: Intracellular pathogens.....	309
2	Methods.....	310
2.1	Bioorthogonal labeling of bacteria and cell infection experiment.....	310
2.2	Fixation and preparation of ultrathin cryo-sections.....	313
2.3	Click reaction and counterstaining of thawed cryo-sections.....	314
2.4	STORM imaging.....	315
2.5	STORM analysis.....	316
2.6	TEM staining.....	316
2.7	TEM imaging and stitching.....	317
2.8	Correlation.....	318
3	Instrumentation and materials.....	319
3.1	Bioorthogonal labeling and cell infection experiments.....	319
3.2	Fixation and preparation of ultrathin cryo-sections.....	319
3.3	Click reaction and counterstaining of thawed cryo-sections.....	319
3.4	Super-resolution microscopy.....	319
3.5	Transmission electron microscopy.....	320
3.6	Correlation.....	320
4	Discussion.....	320
4.1	Flexibility offered by click-chemistry.....	320
4.2	Choice of grids.....	321
4.3	How to correlate.....	321
4.4	Added value of STORM.....	322
4.5	General applicability of the method.....	324
	Acknowledgments.....	324
	References.....	325

Abstract

Correlative light and electron microscopy (CLEM) entails a group of multimodal imaging techniques that are combined to pinpoint to the location of fluorescently labeled molecules in the context of their ultrastructural cellular environment. Here we describe a detailed workflow for STORM-CLEM, in which STochastic Optical Reconstruction Microscopy (STORM), an optical super-resolution technique, is correlated with transmission electron microscopy (TEM). This protocol has the advantage that both imaging modalities have resolution at the nanoscale, bringing higher synergies on the information obtained. The sample is prepared according to the Tokuyasu method followed by click-chemistry labeling and STORM imaging. Then, after heavy metal staining, electron microscopy imaging is performed followed by correlation of the two images. The case study presented here is on intracellular pathogens, but the protocol is versatile and could potentially be applied to many types of samples.

1 Introduction

1.1 CLEM and super-resolution microscopy

Correlative light and electron microscopy (CLEM) is a group of powerful and well-established multimodal imaging techniques in biological research. With these techniques come a wide scope of methodological advances that stems from the ability to place the molecular selectivity of fluorescence microscopy (FM) towards specific proteins and structures, within the subcellular context provided by the high imaging resolution of electron microscopy (EM) (de Boer, Hoogenboom, & Giepmans, 2015). However, between the excellent resolution of EM and that of FM there is a wide gap, that imposes difficulties at the time of correlation.

An evident development in FM is super-resolution microscopy (SRM), a group of far-field optical techniques that are able to bypass Abbe's diffraction limit (Huang, Bates, & Zhuang, 2009; Schermelleh, Heintzmann, & Leonhardt, 2010) and achieve a resolution down to tens of nanometers. These techniques can be divided into three groups: structured illumination microscopy (SIM) (Gustafsson, 2000), stimulated emission depletion (STED) (Hell & Wichmann, 1994), and single-molecule localization microscopy (SMLM) (Nahidiazar, Agronskaia, Broertjes, van den Broek, & Jalink, 2016). SMLM methods overcome the diffraction barrier by ensuring that only a number of emitting particles are in an "on" (emitting) state at a time, whilst the majority are in an "off" (dark) state. The centroid position of each emitter is identified and statistically fitted to a Gaussian, with the localization precision being proportional to the number of photons emitted. By fitting the centroid positions of these emitters over thousands of frames without spatial overlap, a high-resolution image of single molecules can be produced (Fig. 1). SMLM techniques have an excellent resolution (5–25 nm), offer multi-color imaging and can achieve quantification with single-particle precision (Nicovich, Owen, & Gaus, 2017). Direct Stochastic Optical Reconstruction Microscopy (dSTORM) (Heilemann et al., 2008) is one of the most popular choices of SMLM techniques and this is demonstrated through its significant achievements from cellular biology (Xu, Babcock, & Zhuang, 2012) to material science (Pujals, Feiner-Gracia, Delcanale, Voets, & Albertazzi, 2019; van der Zwaag et al., 2016).

1.2 SMLM-CLEM, advantages over conventional CLEM

The past decade has witnessed the rapid rise of SRM techniques and their correlation with EM (SRM-CLEM), amongst others (Hauser et al., 2017). Each correlative method aims to add a new dimension of information, with minimal compromise to image quality and resolution upon correlation. STORM is able to achieve an x-y resolution of about 20 nm and a z resolution of about 50 nm (Jones, Shim, He, & Zhuang, 2011), providing one of the best spatial resolutions in the SMLM group, compatible with that of TEM. Thus, the improved resolution of STORM leads to a nanoscale localization precision of the specific fluorescent labels in the

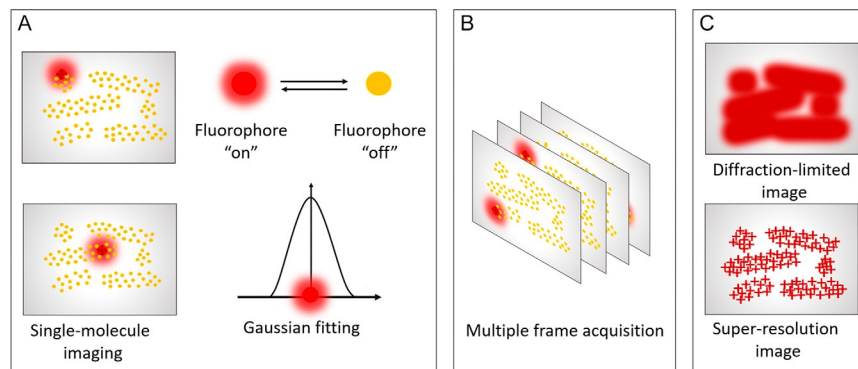


FIG. 1

The principles of STochastic Optical Reconstruction Microscopy (STORM). (A) Only a number of fluorophores are in the “on” (emitting, in red) state at a time, whilst the majority are in the “off” (dark, in yellow) state, allowing the imaging of subsets of fluorophores without spatial overlap and high resolution. The centroid position of each emitter is identified and statistically fitted to a Gaussian. (B) The positions of many emitters are determined over thousands of frames and (C) a super-resolution image is reconstructed from these localizations. The diffraction-limited image is shown in the top right corner as a comparison.

ultrastructural reference space provided by EM (Mateos-Gil, Letschert, Doose, & Sauer, 2016). Importantly, it is a powerful quantitative technique with single-molecule precision (able of molecule counting) (Nicovich et al., 2017). Yet, despite its benefits over conventional CLEM, SRM-CLEM requires sample preparation strategies that agree with both imaging techniques, with minimal compromise to structure and resolution. These strategies focus mainly around the type of fixation and the choice of fluorophore.

1.3 Fixation in SRM-CLEM

It is well-established that chemical fixation and consequent dehydration steps used to preserve ultrastructure in EM can quench fluorescence, and since a strong signal-to-noise ratio is required for the performance of SRM, this step requires careful consideration (Clancy & Cauller, 1998; Watanabe et al., 2011). Metal staining (e.g. using osmium tetroxide) used to enhance the structural contrast can further quench fluorescence, thus some SRM-CLEM studies approach this setback by lowering the osmium tetroxide (OsO_4) concentration during post-fixation (Betzig et al., 2006; Kopek, Shtengel, Xu, Clayton, & Hess, 2012). A more compatible approach is the use of cryo-preparation techniques, such as the Tokuyasu cryo-sectioning method (Tokuyasu, 1986). This was initially developed for immunostaining protocols, but has now been adapted to various CLEM procedures, with or without the need of immunostaining (Cortese, Diaspro, & Tacchetti, 2009; Oorschot, Sztal, Bryson-Richardson, & Ramm, 2014; van Rijnsoever, Oorschot, & Klumperman, 2008).

Although samples are fixed with aldehyde and dehydrated using a cryoprotectant, this approach provides good structural preservation, antibody accessibility, and ease of use. Also, lower concentrations of staining metals can be used as only a thin section (<200 nm) needs to be stained. Another more complicated method for cryopreparation is using high-pressure freezing (HPF) followed by subsequent freeze substitution (FS). This technique provides a very good sample preservation, though at the expense of longer preparation times (McDonald, 2014).

1.4 Fluorescence labeling: Advantages of click chemistry

The power of SRM-CLEM relies in its ability to image specific proteins or structures within cells with a high resolution. Although there are a plethora of approaches to fluorescently label the structures of interest, it is unlikely that one single probe can be suitable for all CLEM protocols (Ando et al., 2018). Standard immunostaining has the advantage of high specificity towards endogenous molecules and avoids problems of probe expression. However, the fixation and permeabilization procedures necessary in the process can cause ultrastructural changes in the sample (Schnell, Dijk, Sjollem, & Giepmans, 2012), and many antibodies are not compatible with thin sections due to insufficient sample penetration or loss of epitope recognition - even when a milder chemical fixation is used such as in Tokuyasu sectioning (Griffiths & Lucocq, 2014; Möbius & Posthuma, 2019).

On the contrary, genetically encoded probes do not require permeabilization to gain entry to structures of interest, thus preserving the membrane structure, and improving the overall quality of EM. Single modality genetic probes (fluorescent proteins) can allow normal photoconversion in heavily fixed resin-embedded samples (OsO₄ 0.5–1%) and are compatible with SRM-CLEM, as in the case of mEos4a (Paez-Segala et al., 2015). Dual modality genetic probes such as miniSOG can convert fluorescent signal to electron dense signal using photoconversion, and preserve fluorescence even after the embedding stage (Ando et al., 2018; Shu et al., 2011). However, the expression levels, fusion position and photophysical properties must be carefully optimized to not disturb biological processes.

Fluorescent proteins (FPs) are often touted for their broad applicability and ease of use but they have clear limitations as well (Jensen, 2012). They remain challenging in specific cases, such as pathogenic organisms, due to risks and license restrictions, or in vivo systems for various ethical and practical reasons. Moreover, even when successfully performed, the fluorescent protein may interfere with the tagged protein, or with the organism as a whole (Jensen, 2012). Another obvious limitation is the fact that FPs can only be used to label proteins, leaving many interesting biomolecules such as peptides, fatty acids, glycans and nucleic acids in the dark. Some of these non-protein biomolecules can be targeted with antibodies but these are highly specialized and suffer from the restrictions as mentioned above (Chan, Lim, MacAry, & Hanson, 2014).

Chemical fluorescent modification with an organic fluorophore represents another way to label biomolecules of interest (Patterson, Nazarova, & Prescher, 2014;

Prescher & Bertozzi, 2005; Sahoo, 2012; Toseland, 2013). This can be done through chemical modification of the building blocks (amino acids, fatty acids, etc.) or direct modification of the macro molecule (proteins, glycans, etc.). Chemical fluorescent tags (~1 kDa) are much smaller than FP tags (~30 kDa), and are generally brighter and suffer from less quenching (Dempsey, Vaughan, Chen, Bates, & Zhuang, 2011). However, these can still severely interfere with the biological function, depending on the modification position, chemical properties of the fluorophore and number of fluorophores per biomolecule (Jensen, 2012; Toseland, 2013). This effect is most pronounced in highly sensitive biological systems such as the immune system (Araman et al., 2018; Hos, Tondini, van Kasteren, & Ossendorp, 2018; Szabó et al., 2018).

Bioorthogonal chemistry—also known as ‘click’ chemistry - uses a two-step labeling mechanism to first introduce a small chemical modification in the biomolecule of interest, followed by a secondary ligation (click) step to attach a fluorophore (or a different reporter) of choice (Prescher & Bertozzi, 2005). The first modification—commonly referred to as click handle—can be as small as a few atoms in size (e.g., $-\text{C}\equiv\text{C}-$ vs $-\text{CH}_3$), minimizing the effect on the biological function (McKay & Finn, 2014). The second step—clicking the fluorophore—can be performed at any time but if chemical fixation is possible or required (as for CLEM), this reaction should be performed afterwards to avoid interference with the biology altogether. This technique can be used to label any biomolecule, provided the structure is synthetically available and large enough to allow a small modification (Prescher & Bertozzi, 2005). Various bioorthogonal reactions have been developed (Devaraj, 2018; Row & Prescher, 2015), that can be chosen based on the requirements of the biological question. The classic copper-catalyzed Huisgen cycloaddition (ccHc) (Rostovtsev, Green, Fokin, & Sharpless, 2002)—or copper-click reaction—involves the ligation of a terminal azide to a terminal alkyne group, catalyzed by copper(I). Either the azide or the alkyne can be incorporated into the biomolecule, depending on synthetic preferences and homology to the natural structure, but the alkyne is preferred due to significantly lower background of the cognate azide-modified fluorophore (Bakkum et al., 2018). This reaction is fast, high yielding and very selective, making it the ideal strategy for two-step labeling of biomolecules involved in sensitive biological processes. The well-known cytotoxicity of copper(I) (Sletten & Bertozzi, 2011) is irrelevant when performing the reaction after chemical fixation but can be avoided using a strain-promoted Huisgen cycloaddition (spHc) reaction, using a cyclooctyne-modified fluorophore (Mateos-Gil et al., 2016).

Not only are these click handles small enough to avoid interfering with the biological processes, they are bioinert (Sletten & Bertozzi, 2011) and (bio)chemically stable (Neef & Luedtke, 2014). This is of great importance when studying immunological processes, that include uptake of foreign material (e.g., bacteria), degradation and processing of the material for antigen presentation. We have previously shown that both the azide and alkyne groups are sufficiently stable to the harsh conditions that occur during degradation of bacteria, to allow the intracellular study of these foreign entities (Bakkum et al., 2018; van Elsland et al., 2016).

1.5 Case study: Intracellular pathogens

The immune system employs a wide range of defensive strategies against foreign invaders, such as viruses, bacteria and multicellular parasites (Murphy & Weaver, 2016). Immune cells sense their presence, process the molecular information and conclude on either a destructive response (clearance) or a non-destructive response (tolerance), to avoid unnecessary damage to the host (McCarville & Ayres, 2018). Bacterial invaders are first internalized through a process called phagocytosis—employed by specialized phagocytic immune cells such as macrophages and dendritic cells—and subsequently killed and degraded in specialized anti-microbial compartments called phagolysosomes (Kinchen & Ravichandran, 2008). Intracellular pathogenic bacteria such as *Salmonella enterica* employ a parasitic lifestyle to avoid killing and clearance by the host cell (Fig. 2) (Fields, Heinzen, & Carabeo, 2011).

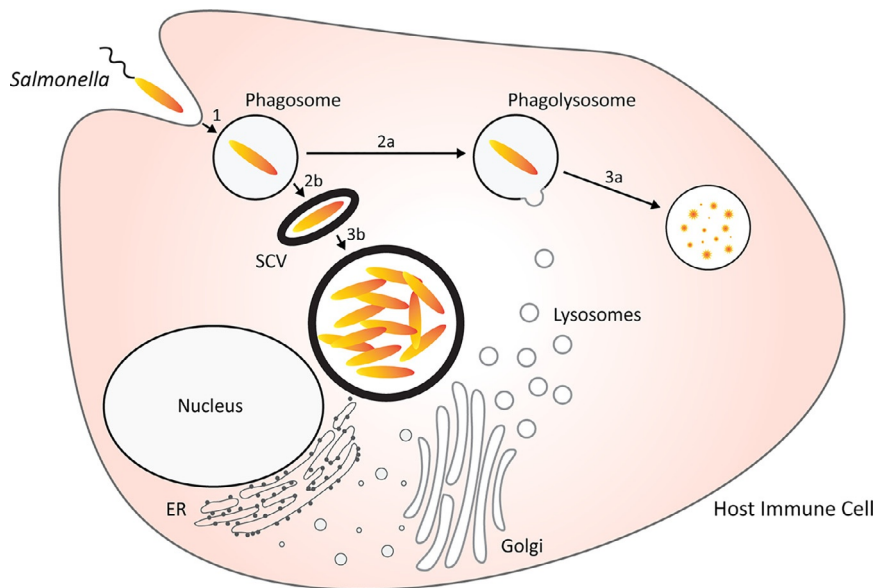


FIG. 2

Simplified schematic representation of the intracellular lifestyle of *Salmonella enterica*. Following uptake by a phagocytic immune cell (**1**), *Salmonella* bacteria initially reside within a host compartment called a phagosome. Phagocytic immune cells are specialized in degrading pathogenic bacteria through fusion of the phagosome with lysosomes (**2a**) to form a highly bactericidal phagolysosome, eventually resulting in the degradation of the pathogen (**3a**). However, *Salmonella* has evolved to evade degradation (**2b**), through the formation of a specialized compartment which is referred to as a *Salmonella*-containing vacuole (SCV). Through this immune-evading strategy, *Salmonella* is able to survive and even multiply freely (**3b**), usually resulting in host cell lysis and spreading of the pathogen.

Classical light and electron microscopy techniques provide insufficient information on the intracellular behavior of pathogenic bacteria, due to the lack of either ultrastructural information, functional information, resolution, or a combination of both. Confocal-CLEM provides both functional information (through click labeling) and ultrastructural information on the subcellular behavior of the pathogen but lacks sufficient resolution to observe the precise label distribution. SRM-CLEM solves this problem and provides additional single-molecule sensitivity, that allows for visualization of sub-bacterial structures and rare events with low label density. We have previously shown that a combination of bioorthogonal labeling, STORM and TEM (STORM-CLEM) provides an effective tool to study the intracellular behavior of *Salmonella enterica* serovar Typhimurium (abbreviated here as *Salmonella*) (van Elsland et al., 2018). The choice of SRM technique stands for achieving the best resolution and using a non-damaging laser power. We found STORM left the sample relatively unaffected, resulting in a well-preserved ultrastructure on EM.

2 Methods

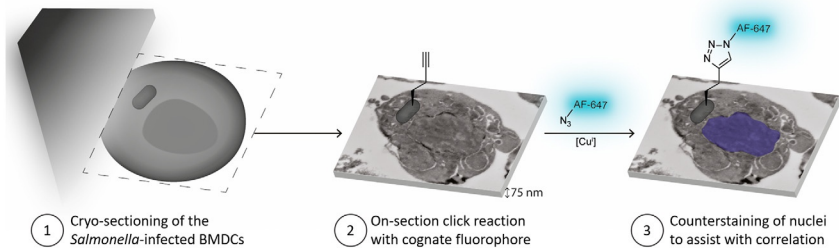
The method described here is primarily focused on the on-section click reaction and subsequent image acquisition and correlation of STORM-CLEM. More details about the original procedure for studying *Salmonella* in murine bone marrow-derived dendritic cells (BMDCs) can be found in the original publication (van Elsland et al., 2018). Tips and alternatives to the protocol are indicated between asterisks (*). Steps that require extra attention or care are indicated between exclamation marks (!). A graphical summary of the protocol is illustrated in Fig. 3 and a simplified workflow with time indications is provided in Fig. 4.

2.1 Bioorthogonal labeling of bacteria and cell infection experiment

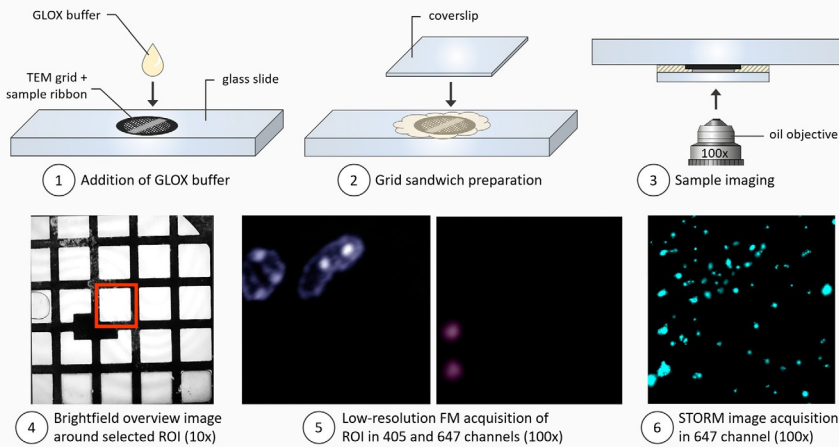
It is strongly recommended to prepare all bacterial and mammalian cells, growth media and reagents beforehand, as the biological experiment requires a strict time schedule. A sufficient number of cells is crucial to obtain a large enough cell pellet for the subsequent sample preparation according to the Tokuyasu method (about 50–100 μ L in volume). Generally, a 10cm cell culture dish with a confluency of >70% should suffice for a single experimental condition (around 5–20 million cells, depending on the cell type).

0. Dilute an overnight culture of *Salmonella* (1:33) and allow to grow back to the exponential growth phase (OD₆₀₀ between 0.3 and 0.5).
1. Replace the growth medium (LB) by a methionine-free alternative (SelenoMet) and supplement with a previously optimized concentration of L-homopropargylglycine (Hpg) (4 mM) for bioorthogonal labeling of the bacterial proteome, according to the BONCAT procedure (Dieterich, Link, Graumann, Tirrell, & Schuman, 2006; Landgraf, Antileo, Schuman, & Dieterich, 2015).

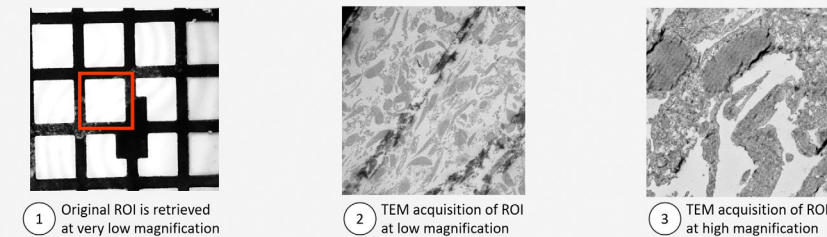
Cryo-sectioning and click reaction with fluorophore



Super-Resolution Microscopy



Electron Microscopy



Correlation of imaging modalities

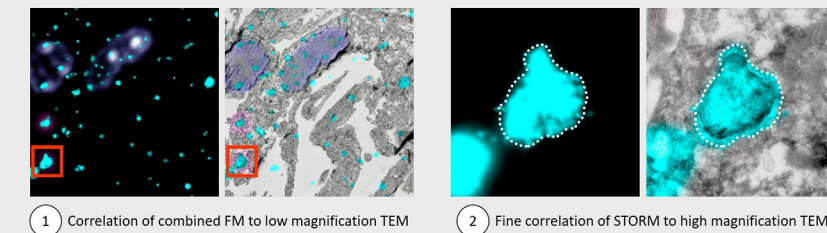
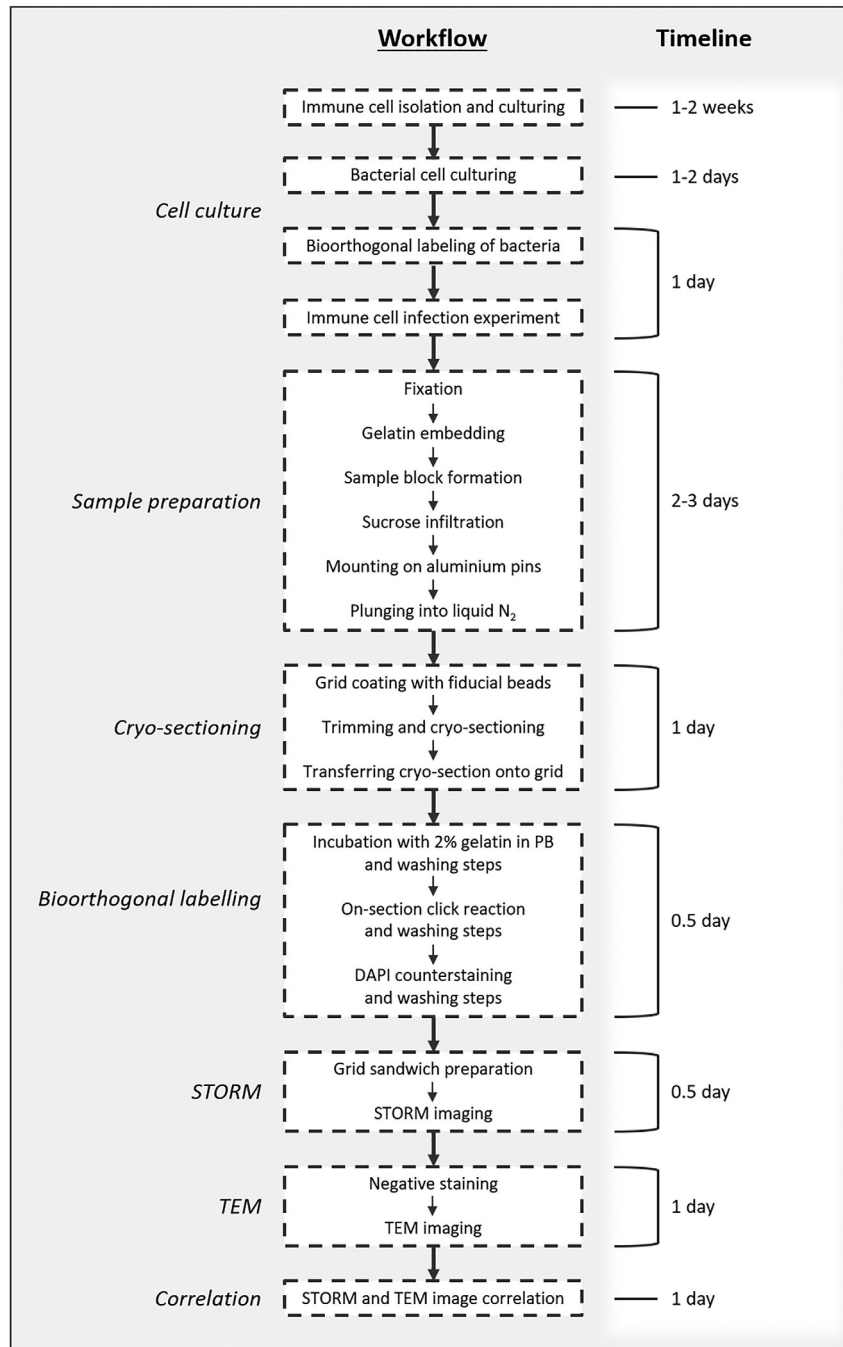


FIG. 3

Graphical summary of the bioorthogonal STORM-CLEM protocol.

**FIG. 4**

Workflow and timeline of the bioorthogonal STORM-CLEM protocol.

(*) The optimal label concentration can be determined by in-gel fluorescence and flow cytometry analysis (van Elsland et al., 2018). Hpg can be easily substituted by L-azidohomoalanine (Aha) if preferred (van Elsland et al., 2016). (*)

2. Incubate the bacteria for approx. 1–2 doubling times (30 min for *Salmonella*).
(*) The effect of label incorporation on bacterial viability can be checked by comparing the growth rates of the bacteria in the presence or absence of the bioorthogonal label (van Elsland et al., 2018). (*)
3. Infect the phagocytic immune cells (BMDCs) by co-incubating with the labeled bacteria (MOI 50) in antibiotic-free cell medium (e.g., IMDM +10% FCS) for 45 min.
4. Wash away the non-internalized bacteria and further incubate the infected cells in medium, according to the biological research question (e.g., 3 h for intracellular processing). Addition of gentamycin (f.c. 100 µg/mL for washes, 10 µg/mL for post-infection incubation) is desirable to kill extracellular bacteria and avoid uncontrolled bacterial growth.

2.2 Fixation and preparation of ultrathin cryo-sections

We previously discovered that the Tokuyasu cryo-sectioning technique is compatible with on-section click reaction (van Elsland et al., 2016), in addition to its well-known compatibility with immunofluorescence (Möbius & Posthuma, 2019; Vicidomini et al., 2008, 2010). Here we briefly describe the method that has been used in the bioorthogonal STORM-CLEM publication, including some updates to the original Tokuyasu method. A complete and comprehensive protocol of the Tokuyasu method, including video tutorials, has been previously published by Peters, Bos, and Griekspoor (2006).

1. Fix the cells directly on the cell culture dish with a f.c. of 2% paraformaldehyde in 0.1 M phosphate buffer pH 7.2 for 24 h at room temperature.
2. Rinse with PBS and 15 mM glycine in PBS to block potential aldehyde residues.
3. Harvest the fixed cells in pre-warmed (37°C) 1% gelatin in PBS using cell scrapers and collect in an Eppendorf tube.
4. Pellet cells by centrifugation for 5 min at 400 rcf and resuspend the pellet in pre-warmed 12% gelatin in PBS.
5. Incubate for 10 min at 37°C, then collect by centrifugation for 3 min at 2500 rcf and solidify gelatin on ice.
6. Cut sample cubes of 0.5–1 mm³ with a razor blade and allow sucrose infiltration by rotating in 2.3 M sucrose in PBS overnight at 4°C.
7. Transfer each sample cube to a metal support pin (to be mounted in the ultramicrotome) and plunge freeze by dropping the pin in a small container filled with liquid nitrogen.
8. Apply fiducials (0.1 µm FluoSpheres) to the Formvar/carbon-coated TEM grid (titanium, 100 square mesh, 3.05 mm, center-marked, Agar Scientific) by incubating the grids for 2 min on a droplet of prediluted (1:10000) and

sonicated (5 min at max power) FluoSpheres. Wash 2×1 min on drops of PBS and 2×1 min on drops of milliQ water. Dry the grids by carefully touching the side of the grid on filter paper and store in a dry grid box until step 15.

9. Mount the sample pin on a cryo-ultramicrotome (Leica UC7 Ultramicrotome equipped with Leica EM FC7 Cryochamber and EM Crion ionizer/charger), pre-cooled to -115°C .
10. Trim the sample cube with a trimming knife (Diatome Trim 20°), leaving behind a block face of approx. $400\ \mu\text{m}$ (h) \times $300\ \mu\text{m}$ (w) \times $50\ \mu\text{m}$ (d) for sectioning.
11. Using a cryo-immuno diamond knife (Diatome Cryo Immuno 35°), cut sequential ultrathin sections of $75\ \text{nm}$ thickness.
12. Guide the growing ribbon with a micromanipulator (Diatome Micromanipulator (LeicaMicrosystems, 2017)) to form a ribbon of 10–20 sections.
13. (!) Pick up the sample ribbon using a metal loop containing a droplet of pickup solution (1.15M sucrose, 1% methylcellulose), making sure the droplet does not freeze before contact with the ribbon is made. (!)
14. Allow the pickup droplet to thaw inside a closed environment such as a $200\ \mu\text{L}$ PCR tube. This avoids condensation from the air, which strongly increases folds in the sample.

(*) Alternatively, a lift-up hinge can be used, as described elsewhere (Bos et al., 2011). (*)
15. Place the droplet (sample down) on a fiducial-coated TEM grid.
16. Place the grid on a droplet of pickup solution (sample down), then place the grid (sample up) in a polyether-covered petri dish and store overnight at 4°C .

2.3 Click reaction and counterstaining of thawed cryo-sections

Various reaction conditions have been suggested and optimized (Hong, Presolski, Ma, & Finn, 2009; Hong, Steinmetz, Manchester, & Finn, 2010; Presolski, Hong, & Finn, 2011) but the conditions described here work robustly in our hands for a wide range of applications, including in-gel fluorescence, flow cytometry, fluorescence microscopy and CLEM. Click reagents should be prepared freshly or stored at -20°C as single-use aliquots. The bioorthogonal reaction mixture (click mix) must be prepared following the indicated order.

1. Place the grid (sample down) on a prewarmed 2% gelatin PBS solution and incubate for 30 min at 37°C .
2. Prepare a clean surface for subsequent washing and staining steps by sticking some Parafilm onto a wet surface and removing the protective film from the top.
3. Prepare droplets of PBS containing 15 mM glycine and use a plastic loop to transfer the grid (sample down) on a droplet, then transfer to a second droplet.
4. Wash 5×2 min on droplets of PBS containing 15 mM glycine.

5. Prepare the click mix in an Eppendorf tube by mixing 4 μ L 0.1 M copper sulfate, 4 μ L 1 M sodium ascorbate, 4 μ L 0.1 M THPTA, 4 μ L 1 M aminoguanidine, 383 μ L 0.1 M HEPES pH 7.4 and 1 μ L 2 mM Alexa Fluor 647-azide (to react to the Hpg-labeled bacteria). Note that the reagents must be added in this sequence to obtain a working reaction mixture.
6. Incubate 60 min on a droplet of click mix.
7. Wash 3 \times 2 min on droplets of PBS.
8. Wash 3 \times 5 min on droplets of PBS containing 1% BSA.
9. Wash 3 \times 2 min on droplets of PBS.
10. Incubate 5 min on a droplet of PBS containing 1 μ g/mL DAPI.
11. Wash 5 \times 2 min on droplets of PBS.

2.4 STORM imaging

The resolution of the confocal microscope is limited to about 250 nm by Abbe's law of diffraction of light, rendering this technique unsuitable for precise imaging of phagocyte-*Salmonella* interactions. STORM is able to circumvent the diffraction barrier and reach an x-y resolution of about 20 nm and a-z resolution of about 50 nm (Jones et al., 2011; Rust, Bates, & Zhuang, 2006), thus has an improved sensitivity of detection of intracellular pathogens and provides a better resolution alignment when used in correlation with TEM. Another important advantage of the STORM-CLEM protocol is that the fluorophore can be introduced after the biological experiment and sample preparation, hence we are not limited by the dyes available to use. We have chosen to label the bacteria using Alexa Fluor 647—one of the best performing cyanine-based STORM dyes—through the cHc ligation method described above. The protocol outlined here is aimed at combining the advantages of STORM and TEM (STORM-CLEM) to study the life cycle of *Salmonella* in BMDCs.

1. GLOX buffer is prepared as described in Materials section.
2. Microscopy slides are pre-cleaned with 100% ethanol and dried using a nitrogen gas flow. The grids containing the sample sections are washed on GLOX droplets (3 \times 5 min) supplemented with 30% glycerol and placed on the glass slide with the thin section facing upwards. A small drop of GLOX buffer (20 μ L) is placed on top of the grid and then covered with a glass coverslip #1.5H (24 mm \times 24 mm, thickness 0.15 mm).
3. Low-magnification images are acquired using the 10 \times objective and the epifluorescence lamp, to map the grid and identify the location of interest in brightfield, 405 channel (nuclei) and 647 channel (bacteria).
4. The 10 \times objective is switched to the 100 \times oil immersion objective and a map is acquired of the area of interest from step 2, using both the transmitted light and fluorescence to specify the reference on the finder grid and the cell position. This will aid in tracing back the same area and cell in TEM.

5. Images are then obtained using the NIKON N-STORM system configured for HILO imaging, using an oil immersive objective (100×). Alexa Fluor 647 is excited using illumination from the 647 laser (160 mW, 1.9 kW cm^{-2}). Fluorescence is collected by means of a Nikon 100×, 1.4 NA oil immersion objective and passed through a quad-band-pass dichroic filter (97,335 Nikon). 20,000 frames at 50 Hz are acquired for the 647 channel. Images are recorded onto a 256×256 pixel region (pixel size 160 nm) of a CMOS camera.
6. STORM images are analyzed with the STORM module of the NIS element Nikon software (van der Zwaag et al., 2016) as described below.

2.5 STORM analysis

Data acquisition and analysis play an important part in the STORM imaging process, and thus detailed protocols should be included in each experiment. As described in Fig. 1, the centroid position of each detected fluorophore is statistically fitted to a Gaussian function, with the precision depending directly on the number of detected photons.

The specific localization of single emitters and the Gaussian fitting is performed using the STORM module in NIS Elements based on the minimum and maximum height parameters. The darkest bright point is selected as the molecule and its brightness minus the background intensity as the minimum height (minimum intensity, 150 in this case). The maximum height possible is 65,000 for a sCMOS camera system, and the baseline 100. The point spread function (PSF) fit width is set to 300, minimum width 200, and maximum width 400. The first 500 frames are discarded due to incomplete photoswitching.

The number of photons per localization is quantified to ensure the reproducibility of the imaging resolution using a protocol elaborated elsewhere (Deschout et al., 2014). The resulting resolution is 20 nm, as expected.

A molecule list is rendered in binary format and the coordinates are translated into an image. This STORM image is either shown in cross or Gaussian mode by the NIKON software. Using cross you can visualize directly all the localizations, whilst Gaussian is a Gaussian rendering of localizations considering lateral localization accuracy (average of $17.9 \pm 4.6 \text{ nm}$) for each localization. In this instance Gaussian mode is used.

2.6 TEM staining

Following STORM acquisition, additional post-staining with uranyl acetate/methyl cellulose is required to create the contrast in TEM and protect the delicate structures. This is done according to the standard Tokuyasu method (Peters et al., 2006), summarized below.

1. The grid containing the sample ribbon is recovered from the microscopy slide, by placing a droplet of PBS next to the coverslip.

2. Using ultra fine tweezers, the coverslip is easily, but very carefully lifted to reveal the grid with the sample on top.
3. The grid is rinsed in ddH₂O and the backside of the grid is dried with compressed air, while holding the sample side of the grid against a droplet of ddH₂O.
4. The sample attached to the grid is washed 5×2 min on droplets of ddH₂O.
5. Droplets of aqueous uranyl acetate (0.4%)/methyl cellulose (1.8%) are placed on clean Parafilm, attached to a plate lid, placed on ice to keep the solution cold.
6. The grid is touched on a droplet, then transferred to another droplet and incubated for 5 min.
7. Using a metal loop, attached to a pipette tip, the grid is recovered from the droplet and the excess uranyl acetate/methyl cellulose is immediately removed by touching the loop sideways on a piece of Whatman 1 filter paper, until only a thin film remains.
8. The grid is air dried for 20 min and can then be stored indefinitely at room temperature.

2.7 TEM imaging and stitching

Manual correlation of different image modalities should ideally be performed step-wise, as it greatly reduces the difficulty of finding the area of interest. An overview image of the TEM grid will provide a non-symmetrical reference for identifying the relevant grid window from which the fluorescence images were acquired. In the same way, an overview image of the grid window will provide a reference for identifying the area of interest from which the high-resolution STORM image was acquired. It is recommended to first correlate the STORM image to the low-resolution fluorescence image, then correlate the combined fluorescence images to a low-magnification ($\sim 200\times$) TEM image, and finally correlating the low-magnification TEM image to a high-magnification ($\sim 11,000\times$) TEM image. An intermediate correlation step with a medium-magnification ($\sim 2000\times$) TEM image is optional but recommended, as it simplifies image registration. Since the field of view (FoV) of FM/STORM is larger than that of TEM at high magnification, it is useful to apply a stitching algorithm to obtain a larger FoV TEM image for correlation.

1. Using a stereoscope, orient the sample grid in the TEM sample holder in the correct way. The final orientation of the grid at the required magnification should correspond to the original orientation during FM/STORM acquisition and can be guided by the asymmetric central marking of the TEM grid. Note that the orientation inside the TEM can change upon increasing magnification, due to the different lenses.
2. At low magnification, identify the grid window that has been imaged by FM/STORM.
3. Acquire a reference TEM image at low magnification ($\sim 200\times$) and use this image to identify the FoV that has been imaged by low res FM. This reference

image can be roughly correlated to the FM/STORM image, to assist in identifying the relevant FoV.

4. Acquire a second reference TEM image/stitch at $\sim 2000\times$ magnification and use this image to identify the FoV that has been imaged by STORM. This reference image can be roughly correlated to the FM/STORM image, to assist in identifying the relevant FoV.
5. Acquire the final TEM image/stitch at high magnification ($\sim 11,000\times$), corresponding approximately to the same FoV that has been imaged by STORM.

2.8 Correlation

All fluorescence images (STORM or low resolution) were pre-processed (brightness/contrast corrected) in ImageJ and exported as RGB color TIF. The low-resolution fluorescence images were first imported into Photoshop as separate layers (overlay mode: Lighten), rasterized and grouped (group overlay mode: Color). Next, the canvas size was increased (e.g., 10-fold) and the high-resolution STORM image was imported as a new top layer (overlay mode: Lighten). The STORM image was transformed (scaling [bicubic interpolation], rotation, translation) to match the low resolution image, based on the available reference landmarks. All layers were grouped (group overlay mode: Color) and the canvas size was increased again (e.g., 10-fold). The TEM image (low magnification or high magnification stitch) was loaded separately into Photoshop. The TEM image was then copied onto the fluorescence images and arranged to the background.

To facilitate correlation of fluorescence to EM, the contrast of the reference markers (nuclear staining and fiducial markers) was temporarily increased (Levels tool), and the grouped fluorescence layers were transformed (scaling [bicubic], rotation, translation) to approximately match the low-magnification ($\sim 200\times$) TEM image. All layers were linked, and the fluorescence layers were hidden, to make EM-to-EM correlation easier. The canvas size was again scaled if required and the next TEM image was imported in the same manner. Correlation of the low-magnification TEM image to the high-magnification TEM image was achieved by reducing the opacity of the top layer (low magnification) and applying transformations to match the high magnification TEM image. The layers were unlinked and the low magnification TEM image hidden. Finally, the grouped fluorescence were unhidden and fine transformations (scaling, rotation, translation) were applied to match the reference landmarks (nuclei and fiducials). Note that image registration should be performed primarily using the available landmarks, to avoid biased correlation of the objects of interest. However, the bacteria described here can be considered as intrinsic landmarks, due to their clear visibility in all image modalities (low resolution fluorescence, STORM and TEM). This means that minor transformations are allowed to match the STORM image to the TEM image more accurately but should be minimized. Ideally, STORM-compatible reference markers should be included to avoid user bias in the correlation (FluoSpheres in our case).

3 Instrumentation and materials

3.1 Bioorthogonal labeling and cell infection experiments

Instrumentation: Bacterial culture facility, cell culture facility, laminar flood cabinet compatible with bacterial infection, OD₆₀₀ spectrophotometer.

Bacteria and mammalian cells: Pathogenic bacteria of interest (*Salmonella enterica* serovar Typhimurium [*Salmonella*] strain SL1344), phagocytic immune cells of interest (murine bone marrow derived dendritic cells [BMDCs] generated from B57BL/6 mice bone marrow).

Materials: Culture flasks, 50 mL Falcon tubes, 10 cm cell culture dishes.

Reagents: Lysogeny Broth (LB), ampicillin, SelenoMet medium (Molecular Dimensions), 400 mM L-methionine (Met), 400 mM L-homopropargylglycine (Hpg), mammalian cell growth medium (IMDM, FCS, GlutaMAX, penicillin, streptomycin, 2-mercaptoethanol, GM-CSF), sterile PBS.

3.2 Fixation and preparation of ultrathin cryo-sections

Instrumentation: 37°C incubator, sonicator bath, stereoscope, Leica UC7 Ultramicrotome equipped with Leica EM FC7 Cryochamber and Leica EM Crion ionizer/charger, Diatome Micromanipulator, Diatome Trim 20° knife, Diatome Cryo Immuno 35° knife.

Materials: Cell scrapers, glass Pasteur pipettes and bulb, single edge and double edge razor blades, ultra-fine tip and regular tweezers, plastic vials with cap, metal support pins, filter paper, liquid nitrogen and Dewar, small container for plunge freezing, glass trimming knife, diamond sectioning knife, Formvar/carbon-coated TEM grids (titanium, 100 square mesh, 3.05 mm, center-marked, Agar Scientific), fiducials (carboxylate-modified blue [350/440] FluoSpheres), metal loop on a handle (with lift-up hinge), 200 µL PCR tubes, 35 mm Petri dishes.

Reagents: fixative (8% aqueous paraformaldehyde [EM-grade] and freshly prepared 0.2 M phosphate buffer pH 7.2 mixed in a ratio of 1:3), 15 mM glycine in PBS, 12% gelatin (type A, bloom 300) in PBS with 0.01% sodium azide, 2.3 M sucrose, 2% methyl cellulose (25 cP).

3.3 Click reaction and counterstaining of thawed cryo-sections

Instrumentation: N.A.

Materials: Parafilm, plastic loop on a handle, 1.5 mL Eppendorf tubes.

Reagents: 0.1 M copper sulfate, 1 M sodium ascorbate, 0.1 M THPTA, 1 M aminoguanidine, 0.1 M HEPES pH 7.4, 2 mM Alexa Fluor 647-azide in DMSO, BSA, 2 mg/mL DAPI solution.

3.4 Super-resolution microscopy

Instrumentation: Nikon N-STORM microscope (100 × oil lens, N.A. = 1.49), system configured for HILO imaging, with a quadband pass dichroic filter (97,335 Nikon) and a Hamamatsu ORCA-Flash 4.0 camera. NIS-Elements Software.

Materials: Glass slides, Coverslip (24 mm × 24 mm, thickness 0.15 mm).

Reagents: GLOX buffer with 30% glycerol: 100 μL PBS, 20 μL 50% glucose, 20 μL MEA 1 M (b-MercaptoEthylamine) and 2 μL GLOX (0.7 mg/mL glucose oxidase, 5 mg/mL catalase in PBS) plus 30% glycerol (60 μL).

3.5 Transmission electron microscopy

Instrumentation: Tecnai 12 Biotwin transmission electron microscope (FEI).

Materials: one metal loop attached to a pipette tip for every grid.

Reagents: uranyl acetate/methyl cellulose (4% uranyl acetate and 2% methyl cellulose [25 cP] mixed in a ratio of 1:9), ddH₂O.

Software: TEM stitching algorithm developed in-house (Faas et al., 2012).

3.6 Correlation

Software: FIJI, Adobe Photoshop CS6 (or higher).

4 Discussion

4.1 Flexibility offered by click-chemistry

As explained in the introduction, click-chemistry allows performing the click reaction on the thawed cryo-sections, thus avoiding reporter interference in the biological process studied. An additional benefit is the freedom to use any clickable fluorophore (or other reporter such as biotin) of choice. Since the number of STORM-compatible fluorophores is limited, this is of major importance. Generally, cyanine-based fluorophores are considered ideal for STORM, due to their high brightness, blinking rate and photon count (Dempsey et al., 2011). When considering clickable fluorophores, an additional consideration should be made in terms of solubility, to minimize non-specific hydrophobic interactions with the sample. This generally steers the selection towards the water-soluble Alexa Fluors, with Alexa Fluor 647 giving the highest blinking rate/photon count (Dempsey et al., 2011). Alternatively, photoactivatable fluorophores for PALM could hypothetically be used as well (Betzig et al., 2006). Other options for fluorescent labeling include the use of a clickable biotin, followed by a separate incubation step with fluorescently modified streptavidin, which may contain an additional gold particle for detection by EM as well (Cheutin et al., 2007; Kurdekar et al., 2018).

Bioorthogonal metabolic labels have been developed for virtually all biomolecules and have so far shown compatibility with nearly all biological systems, including whole animals (Grammel & Hang, 2013). Various mutually-orthogonal bioorthogonal reactions have previously been reported (Liang, Mackey, Lopez, Liu, & Houk, 2012; Patterson & Prescher, 2015; Willems et al., 2012), providing an interesting approach to multiplex labeling and potential multi-color STORM-CLEM. The feasibility and limitations of this approach will depend on the number

of mutually orthogonal reactions, as well as the number of STORM-compatible fluorophores and emission filters available.

Tokuyasu cryo-sections allow fluorophore or gold-modified antibodies as well, to allow multiplex labeling (Möbius & Posthuma, 2019). Although bioorthogonal labeling can be a good alternative for fluorescent proteins, the Tokuyasu method does allow most fluorescent proteins to retain their fluorescence, making them an attractive option to include (ten Brink, Oorschot, & Klumperman, 2015; van Elsland et al., 2016, 2018). Moreover, direct chemical modifications such as fluorescent probes are compatible as well, provided they are fixable (van Meel et al., 2019). However, these must be included in the biological workflow and therefore lack the flexibility of on-section fluorescent labeling. Activity-based probes containing a bioorthogonal group represent a useful alternative for fluorescent probes, maintaining the reporter flexibility after cryo-sectioning (van Elsland et al., 2016).

4.2 Choice of grids

An important aspect to consider in our STORM-CLEM protocol is the choice of grids. Two reasons limit the choice of grids. First, they need to be mounted between a coverslip and a glass slide for STORM imaging and later on they have to be retrieved from it, thus they need to be robust. Second, when performing STORM imaging GLOX buffer is used, so inert metals should be chosen to avoid corrosion. Similarly, copper grids will be affected by the reducing agent of the copper click reaction. For these reasons, we found Titanium grids were the ideal choice for our protocol.

Moreover, we used 100-mesh grids with a non-symmetrical center, as a guide for the correlation. The 100-mesh is just large enough to image one FoV in confocal/low resolution FM and supports the sample to keep it as flat as possible. The non-symmetrical center helps to orient the grid correctly in the TEM and to find the correct window to image.

4.3 How to correlate

The ease of correlation is largely dependent on available reference markers, structural landmarks and/or fiducials, that should be detectable in all imaging modalities (low-resolution FM, super-resolution FM and EM). The most effective markers for the initial coarse correlation are large structures such as nuclei, which can easily be labeled with a fluorescent dye (e.g. DAPI) and are identifiable from low magnification ($\sim 300\times$) TEM. For fine correlation, smaller fiducial markers are required that should be sufficiently spread, as to provide any small area of interest with ideally three fiducials. Various types of fiducials are available, from (multicolor) fluorescent beads (Fu et al., 2019; Tuijtel, Koster, Jakobs, Faas, & Sharp, 2019) to fluorescent gold nanoparticles (Fokkema et al., 2018) and quantum dots (QDots) (Van Hest et al., 2019), each with specific strengths and limitations.

As mentioned before, more accurate correlation could be achieved by introducing SRM-compatible reference markers. The compatibility and accuracy of fiducials depends on their excitation/emission spectra, brightness, photostability and fluorescence lifetime for detection by SRM, and their size and electron density for detection by TEM. QDots have proven to be most broadly compatible with SRM techniques and applicable for CLEM as well (Jin et al., 2018; Killingsworth, Lai, Wu, Yong, & Lee, 2012; Vu, Lam, Hatch, & Lidke, 2015). Fluorescent nanodiamonds (fNDs) have shown great promise for computational SRM or STED-based CLEM, due to their extremely high photostability (Chen, Gaathon, Trusheim, & Englund, 2013; Han et al., 2019; Hsiao, Hui, Tsai, & Chang, 2016; Johnstone, Cairns, & Patton, 2019) and have been used very effectively for multi-color dSTORM (madSTORM) as well (Yi et al., 2016).

4.4 Added value of STORM

In this protocol a bioorthogonal STORM-CLEM approach was used to visualize an intracellular pathogen (*Salmonella*) within the ultrastructural context of a host cell (BMDCs). We previously tested the BONCAT-CLEM method on 75 nm cryosections of *Salmonella* but found that due to the limited resolution of the confocal microscope, the method was not sensitive enough to allow proper imaging of the phagocyte-pathogen interaction (van Elsland et al., 2016). STORM was chosen as it is able to circumvent the diffraction barrier and provide one of the best spatial resolutions and sensitivities in the SMLM group (Jones et al., 2011; Rust et al., 2006). SRM is a fast-evolving addition to CLEM, and since its initial development (Betzig et al., 2006), it is proving to be a true game-changer in overcoming the resolution gap between diffraction-limited FM and EM. In our experiments, STORM left the sample relatively unaffected, resulting in a well-preserved ultrastructure in EM. Several small structures (10–20 nm) were observed surrounding the bacterium, that could not have been detected without the SRM addition to the CLEM technique (van Elsland et al., 2018). Although further scrutiny is required to identify the origin of these structures. They may represent bacterial proteins that have been secreted by *Salmonella*, which is a well-known phenomenon (Anderson & Kendall, 2017; Park et al., 2018; Ramos-Morales, 2012; Steele-Mortimer et al., 2002; Uchiya et al., 1999). The bioorthogonal labeling strategy hypothetically enables the visualization of these secreted proteins, while FP-fusion proteins were shown to be too large to fit through the *Salmonella* secretion system (Van Engelenburg & Palmer, 2010).

The SRM-CLEM technique described here in combination with Tokuyasu cryosectioning demonstrates improved sensitivity of detection of intracellular pathogens, good preservation of dye photoswitching properties and a better resolution alignment when used in correlation with TEM compared to confocal microscopy. Other SRM-CLEM techniques were achieved in literature via different approaches such as lowering the concentrations of OsO₄ during post-fixation and by optimizing the resin embedding step, leading to reduced fluorescence quenching, as reported with PALM (Betzig et al., 2006) and STED with TEM (Watanabe et al., 2011) or SEM (Kopek et al., 2012).

STORM uses highly inclined and laminated optical sheet (HILO) as the standard mode of imaging, an approach that is not limited to imaging the surface of samples as in total internal reflection fluorescence (TIRF). This means that using HILO mode we can achieve an imaging depth of up to 10 μm , with a signal-to-noise ratio only slightly lower than in TIRF. Nevertheless, sample thickness is not an issue for Tokuyasu cryo-sections that are only 75 nm thick, thus serve as excellent biological samples in STORM in either modes.

One of the most remarkable traits of fluorescence microscopy is multi-color imaging, as it enables the determination of colocalization and interaction between different proteins or structures of interest. Through the use of spectrally distinct photoswitchable fluorophores, dSTORM enables multi-color imaging with reduced cross-talk (Bates, Dempsey, Chen, & Zhuang, 2012; Endesfelder et al., 2011; Lampe, Haucke, Sigrist, Heilemann, & Schmoranzler, 2012). Still, although two-color dSTORM has been achieved by imaging different structures using spectrally separated dyes (Feiner-Gracia et al., 2019; van der Zwaag et al., 2016), the limited availability of spectrally different photoswitchable fluorophores hinders the use of more colors. Most organic fluorescent dyes display photoswitching properties, but not all of them meet the criteria required for dSTORM imaging. Generally red fluorophores such as Alexa Fluor 647 and Cy5 perform significantly better than the best-performing dyes in other spectral regions. Therefore, even if one chooses four spectrally different dyes, those in the blue (480–540 nm), yellow (545–600 nm) and NIR (740–805 nm) will be considerably dimmer than those in the red (640–700 nm) spectrum, which may negatively affect the image resolution. It is important to note that in order to improve multi-color imaging, the longer wavelength color (i.e., 647 nm) should be imaged first to reduce the photobleaching caused by the shorter wavelength laser (i.e., 561 nm) due to the overlapping spectra of the two dyes (Xu, Ma, & Liu, 2017).

Moreover, STORM requires aqueous imaging buffers, that typically contain a reducing agent (e.g., β -MercaptoEthylamine/ β -mercaptoethanol) and an oxygen scavenger system (Dempsey et al., 2011). In this protocol we use a mixture of catalase, glucose, and glucose oxidase (GLOX) in combination with a reducing agent (β -MercaptoEthylamine, MEA), in which our chosen fluorophore Alexa Fluor 647 performs best. Unfortunately, different dyes blink optimally in different imaging buffers, hence the multi-color acquisition with STORM is challenging (van de Linde et al., 2011), but possible in 2–3 colors through the use of specific buffers such as Oxyrase/MEA (OxEA) (Nahidiazar et al., 2016). Alternatives to these limitations include sequential labeling and imaging using a single fluorophore (Tam, Cordier, Borbely, Sandoval Álvarez, & Lakadamyali, 2014) or spectral demixing dSTORM (SD-dSTORM), that combines the benefits of red-emitting carbocyanine dyes with spectral demixing (Lampe et al., 2012).

It is important to note that the need for longer image acquisition times in combination with issues arising from the use of imaging buffers – such as acidification of buffer over time affecting the cell integrity (Jones et al., 2011) – can make the study of dynamic processes or live-cell imaging difficult. However, whilst live-cell imaging is a setback for in-vivo experiments, it presents no problem as an imaging tool for

fixed-cell applications as seen in this SRM-CLEM protocol (Dani, Huang, Bergan, Dulac, & Zhuang, 2010; Loschberger et al., 2012; van Elsland et al., 2018).

Furthermore, optimizing the labeling density is a crucial parameter in any STORM protocol. A lower-than-optimal labeling density can have a negative consequence on the image resolution and can augment image artifacts. In this protocol we imaged our 75 nm cryo-sections of *Salmonella* after incubation with Hpg at increasing concentrations (0.04, 0.4 or 4 mM), and found that at 0.04 mM Hpg the signal was too low for the bacteria to be completely reconstructed with STORM.

As previously mentioned, the Tokuyasu cryo-sectioning method was chosen in this protocol as it provides a better structure preservation, molecular diffusivity, and ease of use than the conventional chemical fixation and resin embedding steps. Although originally intended for immunostaining protocols, the two-step nature of our biorthogonal ligations is convenient for Tokuyasu cryo-sectioning, as the click-fluorophore can be introduced after the biological time course and sample preparation, with good diffusivity through the 75 nm cryo-section. Furthermore, by using this technique the STORM imaging buffer can easily access the clicked fluorophores, ensuring optimal photoswitching properties of the dyes.

4.5 General applicability of the method

The presented STORM-CLEM method is applied to the case study of intracellular trafficking of pathogens, but it could potentially be applied to different types of biological samples and could be extended to other types of samples, like synthetic materials, as long they can be fixed and thin-sectioned. As explained, it is a very versatile workflow that could accept many variations: we have described it with clickable dyes, but other types of labeling could also be applied, like immunolabeling, previously labeled structures or fluorescent proteins. When correlating with single-molecule microscopy, the right fluorophore/fluorescent protein should be chosen. Other types of microscopies, like confocal microscopy, STED or SIM could also be implemented.

All in all, we have described a detailed workflow for correlating STORM with TEM on cryo-sections prepared using the Tokuyasu method. Correlating nanoscopic techniques allows access to more detailed information. In the case studied on intracellular pathogens, we could get insights into their intracellular mechanism of invasion. Lastly, click-chemistry labeling allows for freedom on the fluorophore of choice.

Acknowledgments

This work was financially supported by the Ministerio de Economía y Competitividad/ Agencia Estatal de Investigación (AEI) (NANOVAX: EURONANOMED/Acciones de Programación Conjunta Internacional PCIN-2016-025), Spanish Ministry of Science and Innovation (PID2019-109450RB-I00/AEI/10.13039/501100011033), European Research Council/ Horizon 2020 (ERC-StG-757,397), “la Caixa” Foundation (ID 100010434), and by the

Generalitat de Catalunya (2017 SGR 01536) to S.P. and L.A, and NWO Echo (711.015.008) to T.B. and S.I.K. T.A. was supported by a Marie Skłodowska-Curie Horizon 2020 (713673), “la Caixa” Foundation (LCF/BQ/DI18/11660039) fellowship. S.P. is grateful to Prof. J. E. Heuser for his patience and guidance in introducing her to the electron microscopy world.

References

- Anderson, C. J., & Kendall, M. M. (2017). *Salmonella enterica* serovar typhimurium strategies for host adaptation. *Frontiers in Microbiology*, 8, 1–16. <https://doi.org/10.3389/fmicb.2017.01983>.
- Ando, T., Bhamidimarri, S. P., Brending, N., Colin-York, H., Collinson, L., De Jonge, N., et al. (2018). The 2018 correlative microscopy techniques roadmap. *Journal of Physics D: Applied Physics*, 51(44), 443001. <https://doi.org/10.1088/1361-6463/aad055>.
- Araman, C., Pieper-Pournara, L., van Leeuwen, T., Kampstra, A. S. B., Bakkum, T., Marqvorsen, M. H. S., et al. (2018). Bioorthogonal antigens allow the unbiased study of antigen processing and presentation. [Preprint]. *Immunology* <https://doi.org/10.1101/439323>.
- Bakkum, T., van Leeuwen, T., Sarris, A. J. C., van Elsland, D. M., Poulcharidis, D., Overkleeft, H. S., et al. (2018). Quantification of bioorthogonal stability in immune phagocytes using flow cytometry reveals rapid degradation of strained alkynes. *ACS Chemical Biology*, 13(5), 1173–1179. <https://doi.org/10.1021/acscchembio.8b00355>.
- Bates, M., Dempsey, G. T., Chen, K. H., & Zhuang, X. (2012). Multicolor super-resolution fluorescence imaging via multi-parameter fluorophore detection. *ChemPhysChem*, 13(1), 99–107. <https://doi.org/10.1002/cphc.201100735>.
- Betzig, E., Patterson, G. H., Sougrat, R., Lindwasser, O. W., Olenych, S., Bonifacino, J. S., et al. (2006). Imaging intracellular fluorescent proteins at nanometer resolution. *Science*, 313(5793), 1642–1645. <https://doi.org/10.1126/science.1127344>.
- Bos, E., Sant’Anna, C., Gnaegi, H., Pinto, R. F., Ravelli, R. B. G., Koster, A. J., et al. (2011). A new approach to improve the quality of ultrathin cryo-sections; its use for immunogold EM and correlative electron cryo-tomography. *Journal of Structural Biology*, 175(1), 62–72. <https://doi.org/10.1016/j.jsb.2011.03.022>.
- Chan, C. E. Z., Lim, A. P. C., MacAry, P. A., & Hanson, B. J. (2014). The role of phage display in therapeutic antibody discovery. *International Immunology*, 26(12), 649–657. <https://doi.org/10.1093/intimm/dxu082>.
- Chen, E. H., Gaathon, O., Trusheim, M. E., & Englund, D. (2013). Wide-field multispectral super-resolution imaging using spin-dependent fluorescence in nanodiamonds. *Nano Letters*, 13(5), 2073–2077. <https://doi.org/10.1021/nl400346k>.
- Cheutin, T., Sauvage, C., Tchélidzé, P., O’Donohue, M. F., Kaplan, H., Beorchia, A., et al. (2007). Visualizing macromolecules with fluoronanogold: From photon microscopy to electron tomography. *Methods in Cell Biology*, 79(79), 559–574. [https://doi.org/10.1016/S0091-679X\(06\)79022-7](https://doi.org/10.1016/S0091-679X(06)79022-7).
- Clancy, B., & Cauller, L. J. (1998). Reduction of background autofluorescence in brain sections following immersion in sodium borohydride. *Journal of Neuroscience Methods*, 83(2), 97–102. [https://doi.org/10.1016/S0165-0270\(98\)00066-1](https://doi.org/10.1016/S0165-0270(98)00066-1).
- Cortese, K., Diaspro, A., & Tacchetti, C. (2009). Advanced correlative light/electron microscopy: Current methods and new developments using Tokuyasu cryosections. *The Journal of Histochemistry and Cytochemistry*, 57(12), 1103–1112. <https://doi.org/10.1369/jhc.2009.954214>.

- Dani, A., Huang, B., Bergan, J., Dulac, C., & Zhuang, X. (2010). Superresolution imaging of chemical synapses in the brain. *Neuron*, *68*(5), 843–856. <https://doi.org/10.1016/j.neuron.2010.11.021>.
- de Boer, P., Hoogenboom, J. P., & Giepmans, B. N. G. (2015). Correlated light and electron microscopy: Ultrastructure lights up! *Nature Methods*, *12*(6), 503–513. <https://doi.org/10.1038/nmeth.3400>.
- Dempsey, G. T., Vaughan, J. C., Chen, K. H., Bates, M., & Zhuang, X. (2011). Evaluation of fluorophores for optimal performance in localization-based super-resolution imaging. *Nature Methods*, *8*(12), 1027–1040. <https://doi.org/10.1038/nmeth.1768>.
- Deschout, H., Zanicchi, F. C., Mlodzianoski, M., Diaspro, A., Bewersdorf, J., Hess, S. T., et al. (2014). Precisely and accurately localizing single emitters in fluorescence microscopy. *Nature Methods*, *11*(3), 253–266. <https://doi.org/10.1038/nmeth.2843>.
- Devaraj, N. K. (2018). The future of bioorthogonal chemistry [Review-article]. *ACS Central Science*, *4*, 952–959. <https://doi.org/10.1021/acscentsci.8b00251>.
- Dieterich, D. C., Link, A. J., Graumann, J., Tirrell, D. A., & Schuman, E. M. (2006). Selective identification of newly synthesized proteins in mammalian cells using bioorthogonal non-canonical amino acid tagging (BONCAT). *Proceedings of the National Academy of Sciences of the United States of America*, *103*(25), 9482–9487. <https://doi.org/10.1073/pnas.0601637103>.
- Endesfelder, U., Malkusch, S., Flottmann, B., Mondry, J., Liguzinski, P., Verveer, P. J., et al. (2011). Chemically induced photoswitching of fluorescent probes—A general concept for super-resolution microscopy. *Molecules*, *16*(4), 3106–3118. <https://doi.org/10.3390/molecules16043106>.
- Faas, F. G. A., Cristina Avramut, M., van den Berg, B. M., Mieke Mommaas, A., Koster, A. J., & Ravelli, R. B. G. (2012). Virtual nanoscopy: Generation of ultra-large high resolution electron microscopy maps. *Journal of Cell Biology*, *198*(3), 457–469. <https://doi.org/10.1083/jcb.201201140>.
- Feiner-Gracia, N., Olea, R. A., Fitzner, R., El Boujnouni, N., van Asbeck, A. H., Brock, R., et al. (2019). Super-resolution imaging of structure, molecular composition, and stability of single oligonucleotide polyplexes. *Nano Letters*, *19*(5), 2784–2792. <https://doi.org/10.1021/acs.nanolett.8b04407>.
- Fields, K. A., Heinzen, R. A., & Carabeo, R. (2011). The obligate intracellular lifestyle. *Frontiers in Microbiology*, *2*, 1–2. <https://doi.org/10.3389/fmicb.2011.00099>.
- Fokkema, J., Fermie, J., Liv, N., van den Heuvel, D. J., Konings, T. O. M., Blab, G. A., et al. (2018). Fluorescently labelled silica coated gold nanoparticles as fiducial markers for correlative light and electron microscopy. *Scientific Reports*, *8*(1), 13625. <https://doi.org/10.1038/s41598-018-31836-1>.
- Fu, X., Ning, J., Zhong, Z., Ambrose, Z., Charles Watkins, S., & Zhang, P. (2019). AutoCLEM: An automated workflow for correlative live-cell fluorescence microscopy and cryo-electron tomography. *Scientific Reports*, *9*(1), 1–10. <https://doi.org/10.1038/s41598-019-55766-8>.
- Grammel, M., & Hang, H. C. (2013). Chemical reporters for biological discovery. *Nature Chemical Biology*, *9*(8), 475–484. <https://doi.org/10.1038/nchembio.1296>.
- Griffiths, G., & Lucocq, J. M. (2014). Antibodies for immunolabeling by light and electron microscopy: Not for the faint hearted. *Histochemistry and Cell Biology*, *142*(4), 347–360. <https://doi.org/10.1007/s00418-014-1263-5>.
- Gustafsson, M. G. L. (2000). Surpassing the lateral resolution limit by a factor of two using structured illumination microscopy. SHORT COMMUNICATION. *Journal of Microscopy*, *198*(2), 82–87. <https://doi.org/10.1046/j.1365-2818.2000.00710.x>.

- Han, S., Raabe, M., Hodgson, L., Mantell, J., Verkade, P., Lasser, T., et al. (2019). High-contrast imaging of nanodiamonds in cells by energy filtered and correlative light-electron microscopy: toward a quantitative nanoparticle-cell analysis. *Nano Letters*, *19*(3), 2178–2185. <https://doi.org/10.1021/acs.nanolett.9b00752>.
- Hauser, M., Wojcik, M., Kim, D., Mahmoudi, M., Li, W., & Xu, K. (2017). Correlative super-resolution microscopy: New dimensions and new opportunities. *Chemical Reviews*, *117*(11), 7428–7456. <https://doi.org/10.1021/acs.chemrev.6b00604>.
- Heilemann, M., van de Linde, S., Schüttelz, M., Kasper, R., Seefeldt, B., Mukherjee, A., et al. (2008). Subdiffraction-resolution fluorescence imaging with conventional fluorescent probes. *Angewandte Chemie International Edition*, *47*(33), 6172–6176. <https://doi.org/10.1002/anie.200802376>.
- Hell, S. W., & Wichmann, J. (1994). Breaking the diffraction resolution limit by stimulated emission: Stimulated-emission-depletion fluorescence microscopy. *Optics Letters*, *19*(11), 780. <https://doi.org/10.1364/OL.19.000780>.
- Hong, V., Presolski, S. I., Ma, C., & Finn, M. G. (2009). Analysis and optimization of copper-catalyzed azide-alkyne cycloaddition for bioconjugation. *Angewandte Chemie, International Edition*, *48*(52), 9879–9883. <https://doi.org/10.1002/anie.200905087>.
- Hong, V., Steinmetz, N. F., Manchester, M., & Finn, M. G. (2010). Labeling live cells by copper-catalyzed alkyne—azide click chemistry. *Bioconjugate Chemistry*, *21*(10), 1912–1916. <https://doi.org/10.1021/bc100272z>.
- Hos, B. J., Tondini, E., van Kasteren, S. I., & Ossendorp, F. (2018). Approaches to improve chemically defined synthetic peptide vaccines. *Frontiers in Immunology*, *9*, 884. <https://doi.org/10.3389/fimmu.2018.00884>.
- Hsiao, W. W. W., Hui, Y. Y., Tsai, P. C., & Chang, H. C. (2016). Fluorescent nanodiamond: A versatile tool for long-term cell tracking, super-resolution imaging, and nanoscale temperature sensing. *Accounts of Chemical Research*, *49*(3), 400–407. <https://doi.org/10.1021/acs.accounts.5b00484>.
- Huang, B., Bates, M., & Zhuang, X. (2009). Super-resolution fluorescence microscopy. *Annual Review of Biochemistry*, *78*(1), 993–1016. <https://doi.org/10.1146/annurev.biochem.77.061906.092014>.
- Jensen, E. C. (2012). Use of fluorescent probes: Their effect on cell biology and limitations. *Anatomical Record*, *295*(12), 2031–2036. <https://doi.org/10.1002/ar.22602>.
- Jin, D., Xi, P., Wang, B., Zhang, L., Enderlein, J., & Oijen, A. M. V. (2018). Nanoparticles for super-resolution microscopy and single-molecule tracking. *Nature Methods*, *15*, 1–10. <https://doi.org/10.1038/s41592-018-0012-4>.
- Johnstone, G. E., Cairns, G. S., & Patton, B. R. (2019). Nanodiamonds enable adaptive-optics enhanced, super-resolution, twophoton excitation microscopy. *Royal Society Open Science*, *6*(7), 190589. <https://doi.org/10.1098/rsos.190589>.
- Jones, S. A., Shim, S.-H., He, J., & Zhuang, X. (2011). Fast, three-dimensional super-resolution imaging of live cells. *Nature Methods*, *8*(6), 499–505. <https://doi.org/10.1038/nmeth.1605>.
- Killingsworth, M. C., Lai, K., Wu, X., Yong, J. L. C., & Lee, C. S. (2012). Quantum dot immunocytochemical localization of somatostatin in somatostatinoma by wide-field epifluorescence, superresolution light, and immunoelectron microscopy. *Journal of Histochemistry and Cytochemistry*, *60*(11), 832–843. <https://doi.org/10.1369/0022155412459856>.
- Kinchen, J. M., & Ravichandran, K. S. (2008). Phagosome maturation: Going through the acid test. *Nature Reviews Molecular Cell Biology*, *9*(10), 781–795. <https://doi.org/10.1038/nrm2515>.

- Kopeck, B. G., Shtengel, G., Xu, C. S., Clayton, D. A., & Hess, H. F. (2012). Correlative 3D superresolution fluorescence and electron microscopy reveal the relationship of mitochondrial nucleoids to membranes. *Proceedings of the National Academy of Sciences of the United States of America*, 109(16), 6136–6141. <https://doi.org/10.1073/pnas.1121558109>.
- Kurdekar, A. D., Chunduri, L. A. A., Manohar, C. S., Haleyrigirisetty, M. K., Hewlett, I. K., & Venkataramaniah, K. (2018). Streptavidin-conjugated gold nanoclusters as ultrasensitive fluorescent sensors for early diagnosis of HIV infection. *Science Advances*, 4(11), 1–11. <https://doi.org/10.1126/sciadv.aar6280>.
- Lampe, A., Haucke, V., Sigrist, S. J., Heilemann, M., & Schmoranzler, J. (2012). Multi-colour direct STORM with red emitting carbocyanines. *Biology of the Cell*, 104(4), 229–237. <https://doi.org/10.1111/boc.201100011>.
- Landgraf, P., Antileo, E. R., Schuman, E. M., & Dieterich, D. C. (2015). BONCAT: Metabolic labeling, click chemistry, and affinity purification of newly synthesized proteomes. *Methods in Molecular Biology*, 1266, 199–215. https://doi.org/10.1007/978-1-4939-2272-7_14.
- LeicaMicrosystems (2017). *Double micromanipulator for cryo-ultramicrotomy—YouTube*. Retrieved 4 May 2020, from <https://www.youtube.com/watch?v=wy1F0oEskkk>.
- Liang, Y., Mackey, J. L., Lopez, S. A., Liu, F., & Houk, K. N. (2012). Control and design of mutual orthogonality in bioorthogonal cycloadditions. *Journal of the American Chemical Society*, 134(43), 17904–17907. <https://doi.org/10.1021/ja309241e>.
- Loschberger, A., van de Linde, S., Dabauvalle, M.-C., Rieger, B., Heilemann, M., Krohne, G., et al. (2012). Super-resolution imaging visualizes the eightfold symmetry of gp210 proteins around the nuclear pore complex and resolves the central channel with nanometer resolution. *Journal of Cell Science*, 125(3), 570–575. <https://doi.org/10.1242/jcs.098822>.
- Mateos-Gil, P., Letschert, S., Doose, S., & Sauer, M. (2016). Super-resolution imaging of plasma membrane proteins with click chemistry. *Frontiers in Cell and Developmental Biology*, 4, 1–16. <https://doi.org/10.3389/fcell.2016.00098>.
- McCarville, J., & Ayres, J. (2018). Disease tolerance: Concept and mechanisms. *Current Opinion in Immunology*, 50, 88–93. <https://doi.org/10.1016/j.physbeh.2017.03.040>.
- McDonald, K. L. (2014). Rapid embedding methods into epoxy and LR white resins for morphological and immunological analysis of cryofixed biological specimens. *Microscopy and Microanalysis*, 20(1), 152–163. <https://doi.org/10.1017/S1431927613013846>.
- McKay, C. S., & Finn, M. G. (2014). Click chemistry in complex mixtures: Bioorthogonal bioconjugation. *Chemistry & Biology*, 21(9), 1075–1101. <https://doi.org/10.1016/j.chembiol.2014.09.002>.
- Möbius, W., & Posthuma, G. (2019). Sugar and ice: Immunoelectron microscopy using cryosections according to the Tokuyasu method. *Tissue and Cell*, 57, 90–102. <https://doi.org/10.1016/j.tice.2018.08.010>.
- Murphy, K., & Weaver, C. (2016). *Janeway's immunobiology*, Garland Science, ISBN: 978-0-815-34550-3.
- Nahidiazar, L., Agronskaia, A. V., Broertjes, J., van den Broek, B., & Jalink, K. (2016). Optimizing imaging conditions for demanding multi-color super resolution localization microscopy. *PLoS One*, 11(7), e0158884. <https://doi.org/10.1371/journal.pone.0158884>.
- Neef, A. B., & Luedtke, N. W. (2014). An azide-modified nucleoside for metabolic labeling of DNA. *Chembiochem*, 15(6), 789–793. <https://doi.org/10.1002/cbic.201400037>.

- Nicovich, P. R., Owen, D. M., & Gaus, K. (2017). Turning single-molecule localization microscopy into a quantitative bioanalytical tool. *Nature Protocols*, *12*(3), 453–460. <https://doi.org/10.1038/nprot.2016.166>.
- Oorschot, V. M. J., Sztal, T. E., Bryson-Richardson, R. J., & Ramm, G. (2014). Immuno-correlative light and electron microscopy on Tokuyasu cryosections. In *Vol. 124. Methods in cell biology* (pp. 241–258). Elsevier. <https://doi.org/10.1016/B978-0-12-801075-4.00011-2>.
- Paez-Segala, M. G., Sun, M. G., Shtengel, G., Viswanathan, S., Baird, M. A., Macklin, J. J., et al. (2015). Fixation-resistant photoactivatable fluorescent proteins for CLEM. *Nature Methods*, *12*(3), 215–218. <https://doi.org/10.1038/nmeth.3225>.
- Park, D., Lara-Tejero, M., Waxham, M. N., Li, W., Hu, B., Galán, J. E., et al. (2018). Visualization of the type III secretion mediated Salmonella-host cell interface using cryo-electron tomography. *eLife*, *7*, e39514. <https://doi.org/10.7554/eLife.39514>.
- Patterson, D. M., Nazarova, L. A., & Prescher, J. A. (2014). Finding the right (bio)orthogonal chemistry. *ACS Chemical Biology*, *9*(3), 592–605. <https://doi.org/10.1021/cb400828a>.
- Patterson, D. M., & Prescher, J. A. (2015). Orthogonal bioorthogonal chemistries. *Current Opinion in Chemical Biology*, *28*, 141–149. <https://doi.org/10.1016/j.cbpa.2015.07.006>.
- Peters, P. J., Bos, E., & Griekspoor, A. (2006). Cryo-immunogold electron microscopy. *Current Protocols in Cell Biology*, *30*(1), 4.7.1–4.7.19. <https://doi.org/10.1002/0471143030.cb0407s30>.
- Prescher, J. a., & Bertozzi, C. R. (2005). Chemistry in living systems. *Nature Chemical Biology*, *1*(1), 13–21. <https://doi.org/10.1038/nchembio0605-13>.
- Presolski, S. L., Hong, V. P., & Finn, M. G. (2011). Copper-catalyzed azide–alkyne click chemistry for bioconjugation. *Current Protocols in Chemical Biology*, *3*(4), 153–162. <https://doi.org/10.1002/9780470559277.ch110148.Copper-Catalyzed>.
- Pujals, S., Feiner-Gracia, N., Delcanale, P., Voets, I., & Albertazzi, L. (2019). Super-resolution microscopy as a powerful tool to study complex synthetic materials. *Nature Reviews Chemistry*, *3*(2), 68–84. <https://doi.org/10.1038/s41570-018-0070-2>.
- Ramos-Morales, F. (2012). Impact of *Salmonella enterica* type III secretion system effectors on the eukaryotic host cell. *ISRN Cell Biology*, *2012*, 1–36. <https://doi.org/10.5402/2012/787934>.
- Rostovtsev, V. V., Green, L. G., Fokin, V. V., & Sharpless, K. B. (2002). A stepwise huisgen cycloaddition process: Copper(I)-catalyzed regioselective ‘ligation’ of azides and terminal alkynes. *Angewandte Chemie, International Edition*, *41*(14), 2596–2599. [https://doi.org/10.1002/1521-3773\(20020715\)41:14<2596::AID-ANIE2596>3.0.CO;2-4](https://doi.org/10.1002/1521-3773(20020715)41:14<2596::AID-ANIE2596>3.0.CO;2-4).
- Row, R. D., & Prescher, J. A. (2015). Constructing new bioorthogonal reagents and reactions. *Accounts of Chemical Research*, *51*(5), 1073–1081. <https://doi.org/10.1016/j.physbeh.2017.03.040>.
- Rust, M. J., Bates, M., & Zhuang, X. (2006). Sub-diffraction-limit imaging by stochastic optical reconstruction microscopy (STORM). *Nature Methods*, *3*(10), 793–796. <https://doi.org/10.1038/nmeth929>.
- Sahoo, H. (2012). Fluorescent labeling techniques in biomolecules: A flashback. *RSC Advances*, *2*(18), 7017–7029. <https://doi.org/10.1039/c2ra20389h>.
- Schermelleh, L., Heintzmann, R., & Leonhardt, H. (2010). A guide to super-resolution fluorescence microscopy. *The Journal of Cell Biology*, *190*(2), 165–175. <https://doi.org/10.1083/jcb.201002018>.

- Schnell, U., Dijk, F., Sjollem, K. A., & Giepmans, B. N. G. (2012). Immunolabeling artifacts and the need for live-cell imaging. *Nature Methods*, 9(2), 152–158. <https://doi.org/10.1038/nmeth.1855>.
- Shu, X., Lev-Ram, V., Deerinck, T. J., Qi, Y., Ramko, E. B., Davidson, M. W., et al. (2011). A genetically encoded tag for correlated light and electron microscopy of intact cells, tissues, and organisms. *PLoS Biology*, 9(4), e1001041. <https://doi.org/10.1371/journal.pbio.1001041>.
- Slatten, E. M., & Bertozzi, C. R. (2011). From mechanism to mouse; a tale of two bioorthogonal reactions. *Accounts of Chemical Research*, 44(9), 666–676. <https://doi.org/10.1021/ar200148z>.
- Steele-Mortimer, O., Brumell, J. H., Knodler, L. A., Méresse, S., Lopez, A., & Finlay, B. B. (2002). The invasion-associated type III secretion system of *Salmonella enterica* serovar Typhimurium is necessary for intracellular proliferation and vacuole biogenesis in epithelial cells. *Cellular Microbiology*, 4(1), 43–54. <https://doi.org/10.1046/j.1462-5822.2002.00170.x>.
- Szabó, Á., Szendi-Szatmári, T., Ujlaky-Nagy, L., Rádi, I., Vereb, G., Szöllösi, J., et al. (2018). The effect of fluorophore conjugation on antibody affinity and the photophysical properties of dyes. *Biophysical Journal*, 114(3), 688–700. <https://doi.org/10.1016/j.bpj.2017.12.011>.
- Tam, J., Cordier, G. A., Borbely, J. S., Sandoval Álvarez, Á., & Lakadamyali, M. (2014). Cross-talk-free multi-color STORM imaging using a single fluorophore. *PLoS One*, 9(7), e101772. <https://doi.org/10.1371/journal.pone.0101772>.
- ten Brink, C., Oorschot, V., & Klumperman, J. (2015). Correlative light and Electron microscopy (CLEM) on biological samples using immuno electron microscopy. *Microscopy and Microanalysis*, 21(S3), 1379–1380. <https://doi.org/10.1017/S1431927615007680>.
- Tokuyasu, K. T. (1986). Application of cryoultramicrotomy to immunocytochemistry. *Journal of Microscopy*, 143(2), 139–149. <https://doi.org/10.1111/j.1365-2818.1986.tb02772.x>.
- Toseland, C. P. (2013). Fluorescent labeling and modification of proteins. *Journal of Chemical Biology*, 6(3), 85–95. <https://doi.org/10.1007/s12154-013-0094-5>.
- Tuijtel, M. W., Koster, A. J., Jakobs, S., Faas, F. G. A., & Sharp, T. H. (2019). Correlative cryo super-resolution light and electron microscopy on mammalian cells using fluorescent proteins. *Scientific Reports*, 9(1), 1369. <https://doi.org/10.1038/s41598-018-37728-8>.
- Uchiya, K., Barbieri, M. A., Funato, K., Shah, A. H., Stahl, P. D., & Groisman, E. A. (1999). A *Salmonella* virulence protein that inhibits cellular trafficking. *The EMBO Journal*, 18(14), 3924–3933.
- van de Linde, S., Löschberger, A., Klein, T., Heidbreder, M., Wolter, S., Heilemann, M., et al. (2011). Direct stochastic optical reconstruction microscopy with standard fluorescent probes. *Nature Protocols*, 6(7), 991–1009. <https://doi.org/10.1038/nprot.2011.336>.
- van der Zwaag, D., Vanparijs, N., Wijnands, S., De Rycke, R., De Geest, B. G., & Albertazzi, L. (2016). Super resolution imaging of nanoparticles cellular uptake and trafficking. *ACS Applied Materials & Interfaces*, 8(10), 6391–6399. <https://doi.org/10.1021/acsami.6b00811>.
- van Elsland, D. M., Bos, E., de Boer, W., Overkleeft, H. S., Koster, A. J., & van Kasteren, S. I. (2016). Detection of bioorthogonal groups by correlative light and electron microscopy allows imaging of degraded bacteria in phagocytes. *Chemical Science*, 7(1), 752–758. <https://doi.org/10.1039/C5SC02905H>.

- van Elsland, D. M., Pujals, S., Bakkum, T., Bos, E., Oikonomeas-Koppas, N., Berlin, I., et al. (2018). Ultrastructural imaging of Salmonella–host interactions using super-resolution correlative light-electron microscopy of bioorthogonal pathogens. *ChemBiochem*, 19(16), 1766–1770. <https://doi.org/10.1002/cbic.201800230>.
- Van Engelenburg, S. B., & Palmer, A. E. (2010). Imaging type-III secretion reveals dynamics and spatial segregation of Salmonella effectors. *Nature Methods*, 7(4), 325–330. <https://doi.org/10.1038/nmeth.1437>.
- Van Hest, J. J. H. A., Agronskaia, A. V., Fokkema, J., Montanarella, F., Gregorio Puig, A., De Mello Donega, C., et al. (2019). Towards robust and versatile single nanoparticle fiducial markers for correlative light and electron microscopy. *Journal of Microscopy*, 274(1), 13–22. <https://doi.org/10.1111/jmi.12778>.
- van Meel, E., Bos, E., van der Lienden, M. J. C., Overkleeft, H. S., van Kasteren, S. I., Koster, A. J., et al. (2019). Localization of active endogenous and exogenous β -glucocerebrosidase by correlative light-electron microscopy in human fibroblasts. *Traffic*, 20(5), 346–356. <https://doi.org/10.1111/tra.12641>.
- van Rijnsoever, C., Oorschot, V., & Klumperman, J. (2008). Correlative light-electron microscopy (CLEM) combining live-cell imaging and immunolabeling of ultrathin cryosections. *Nature Methods*, 5(11), 973–980. <https://doi.org/10.1038/nmeth.1263>.
- Vicidomini, G., Gagliani, M. C., Canfora, M., Cortese, K., Frosi, F., Santangelo, C., et al. (2008). High data output and automated 3D correlative light-electron microscopy method. *Traffic*, 9(11), 1828–1838. <https://doi.org/10.1111/j.1600-0854.2008.00815.x>.
- Vicidomini, G., Gagliani, M. C., Cortese, K., Krieger, J., Buescher, P., Bianchini, P., et al. (2010). A novel approach for correlative light electron microscopy analysis. *Microscopy Research and Technique*, 73(3), 215–224. <https://doi.org/10.1002/jemt.20777>.
- Vu, T. Q., Lam, W. Y., Hatch, E. W., & Lidke, D. S. (2015). Quantum dots for quantitative imaging: From single molecules to tissue. *Cell and Tissue Research*, 360(1), 71–86. <https://doi.org/10.1007/s00441-014-2087-2>.
- Watanabe, S., Punge, A., Hollopeter, G., Willig, K. I., Hobson, R. J., Davis, M. W., et al. (2011). Protein localization in electron micrographs using fluorescence nanoscopy. *Nature Methods*, 8(1), 80–84. <https://doi.org/10.1038/nmeth.1537>.
- Willems, L. I., Li, N., Florea, B. I., Ruben, M., Van Der Marel, G. A., & Overkleeft, H. S. (2012). Triple bioorthogonal ligation strategy for simultaneous labeling of multiple enzymatic activities. *Angewandte Chemie, International Edition*, 51(18), 4431–4434. <https://doi.org/10.1002/anie.201200923>.
- Xu, K., Babcock, H. P., & Zhuang, X. (2012). Dual-objective STORM reveals three-dimensional filament organization in the actin cytoskeleton. *Nature Methods*, 9(2), 185–188. <https://doi.org/10.1038/nmeth.1841>.
- Xu, J., Ma, H., & Liu, Y. (2017). Stochastic optical reconstruction microscopy (STORM). *Current Protocols in Cytometry*, 81(1), 12.46.1–12.46.27. <https://doi.org/10.1002/cpcy.23>.
- Yi, J., Manna, A., Barr, V. A., Hong, J., Neuman, K. C., & Samelson, L. E. (2016). MadSTORM: A superresolution technique for large-scale multiplexing at single-molecule accuracy. *Molecular Biology of the Cell*, 27(22), 3591–3600. <https://doi.org/10.1091/mbc.E16-05-0330>.